

Contents lists available at ScienceDirect

Deep-Sea Research Part I

journal homepage: www.elsevier.com/locate/dsri





Time series of hydrothermal vent fluid chemistry at Main Endeavour Field, Juan de Fuca Ridge: Remote sampling using the NEPTUNE cabled observatory

William E. Seyfried Jr. ^a, Chunyang Tan ^a, Xun Wang ^b, Shijun Wu ^b, Guy N. Evans ^{a,*}, Laurence A. Coogan ^c, Steven F. Mihály ^d, Marvin D. Lilley ^e

- ^a Department of Earth and Environmental Sciences, University of Minnesota, Minneapolis, MN, 55455, USA
- ^b State Key Laboratory of Fluid Power and Mechatronic Systems, Zhejiang University, Hangzhou, 310027, China
- ^c School of Earth and Ocean Sciences, University of Victoria, Victoria, British Columbia, Canada
- ^d Ocean Networks Canada, University of Victoria Queenswood Campus, British Columbia, Canada
- ^e School of Oceanography, University of Washington, Seattle, WA, 98195, USA

ARTICLE INFO

Keywords:
Seafloor hydrothermal vents
Cabled array
Remote sampling
Main Endeavour Field
Ocean Networks Canada

ABSTRACT

Seafloor hydrothermal fluids play a critical role in regulating a wide range of geochemical and biological processes. Chemical and physical changes to venting fluids undoubtedly occur in response to geological events, at depth or near the seafloor, with corresponding effects on vent fluid chemistry, mineralization, and biological activity. However, the uncertain timing of such events makes it impractical to anticipate their occurrence. Thus, the temporal evolution of seafloor vent fluids and coexisting mineral deposits is most often inferred from observations made using conventional deep submergence assets that may be non-continuous for a specific vent field. The recent development of submarine volcanic observatories operated by Ocean Networks Canada (ONC) and the Ocean Observatory Initiative (OOI) in the U.S. that deliver power to instruments on the seafloor and communications via high-speed fiber optic cable permits real-time communication and monitoring of seafloor vents. Here, we describe the development and application of a remotely operated hydrothermal fluid sampler that enables repeat on-demand sampling of high-temperature vent fluids triggered through the internet. The sampler was deployed from September 2019 to June 2020 at the S&M vent area, in the southern portion of Main Endeavour Field (MEF), Juan de Fuca Ridge, on ONC's NEPTUNE ocean observatory. Nine vent fluid samples were acquired over a period of nine months. Analyses of these samples confirm the moderately high-temperature origin of the source fluid, as indicated, for example, by dissolved chloride depletion relative to seawater (vaporrich) and moderately high silica concentrations. These and other dissolved species, such as methane, a known hallmark of MEF vent fluids, are in excellent agreement with the reported composition of S&M vent fluids over the past 15 years or more, suggesting overall chemical stability and rock-dominated alteration processes. On the other hand, short-term variability of dissolved Mg, sulfate and barium indicate entrainment of conductively heated and partially reacted seawater. Both before and after the incursion of the "secondary" seawater derived fluid, however, samples reveal the lowest Mg and sulfate concentrations yet reported for seafloor hydrothermal vent fluid samples. Accordingly, these data provide new insight on the solubility of these and other elements coexisting with minerals close to the Axial Magma Chamber (AMC), from which the primary source fluid is ultimately derived. A separate noteworthy event characterized by $\sim\!20\,^{\circ}\text{C}$ decrease in temperature and associated 24-77% decrease in dissolved Fe concentration was observed toward the end of the deployment, with implications for hydrothermal transition metal fluxes and linked biogeochemical processes. On-demand remote acquisition of a continuous series of high-temperature vent fluid samples from a single vent permits the temporal evolution of heat and mass transfer processes to be studied with a heretofore unavailable perspective. Furthermore, deployment of this sampler within the NEPTUNE ocean observatory opens the door to future studies based on comparative analysis of contemporaneous datasets.

E-mail address: gevans@umn.edu (G.N. Evans).

^{*} Corresponding author. 116 Church St. SE, John Tate Hall, Department of Earth and Environmental Sciences, University of Minnesota, Minneapolis, MN, 55455, USA.

1. Introduction

Hydrothermal alteration processes at mid-ocean ridges have been long recognized to play a key role in heat and mass transfer processes, with implications for the chemical evolution of the ocean and ocean crust (Butterfield et al., 1994; Coogan et al., 2019; Elderfield and Schultz, 1996; German and Seyfried, 2014; Von Damm, 2000). Although it can be anticipated that geological phenomena of the type that drives hydrothermal activity operate on relatively long-time scales, more abrupt changes in crustal permeability can result in equally abrupt variations in the chemistry of vent fluids collected at the seafloor (Sohn et al., 1998; Von Damm et al., 2003). Often associated with these geophysically induced triggering events, phase separation of an initially homogeneous NaCl-fluid of seawater origin can occur, accounting for the formation of vapor and brine components characterized by fundamentally different transport properties of aqueous species (Coogan et al., 2019; Coumou et al., 2008; Driesner and Heinrich, 2007; Foustoukos and Seyfried, 2007; Geiger et al., 2006; German and Seyfried, 2014; Ingebritsen et al., 2010).

Owing to the likelihood that geological events lead to linked geochemical and biological variability in seafloor hydrothermal vent systems, monitoring efforts were initiated, beginning in earnest with the U.S. NSF R2K program. These efforts largely involved time-series investigations of hydrothermal processes on the East Pacific Rise at 9 °N (Edwards et al., 2001; Fornari et al., 2012; Shank et al., 1998; Tolstoy et al., 2006, 2008; Von Damm, 1995, 2000) and at the Endeavour Segment of the Juan de Fuca Ridge (Hooft et al., 2010; Kelley et al., 2012; Wilcock et al., 2009; Wilcock and McNabb, 1996). Repeated return on a near annual time scale to so-called "focus sites" at the respective ridges constituted an essential component of this initiative, where integrated geochemical, biological and geophysical studies could be performed, with an emphasis on linking deep crustal processes to vent related phenomena, especially vent fluid chemistry and biological activity (Fornari et al., 2012; Kelley et al., 2012; Lilley et al., 2003; Mullineaux et al., 2003; Shank et al., 1994; Tolstoy et al., 2008; Von Damm et al., 1997; Von Damm and Lilley, 2004). Importantly, diking events (MEF) and seafloor eruptions (EPR 9°N) occurred during the time of the R2K program, providing a wealth of information, particularly on the feedback between magmatic processes and corresponding changes in hydrothermal and biological activity (Fornari et al., 2012; Kelley et al., 2012; Lilley et al., 2003; Lutz et al., 1994; Mullineaux et al., 2010; Seyfried et al., 2003; Von Damm et al., 2003; Von Damm and Lilley, 2004; Wilcock et al., 2002).

The potential for changes in hydrothermal and linked biological activity at deep sea vents motivated the development and construction of ocean observatories to assess temporal evolution on a higherresolution time scale (Chave et al., 2004; Chen et al., 2012; Isern and Clark, 2003). The Ocean Networks Canada (ONC) and U.S Ocean Observatory Initiative (OOI) are examples of fully functioning facilities that provide unprecedented amounts of power and two-way communications bandwidth to access and control instrument networks in the ocean, while also demonstrating the reliability and functionality of monitoring instrumentation that can complement traditional, ship-based, expeditionary science (Delaney et al., 1987, 2001; Kelley et al., 2014). Cabled ocean observatories are designed around submarine fiber optic/power cables that connect one or more seafloor science nodes to the terrestrial power grid and communications systems. The present report describes the results of the deployment of a novel vent fluid sampling system that takes full advantage of the seafloor fiber optic networks and shore-based infrastructure intrinsic to the NEPTUNE ocean observatory, operated and maintained by ONC. A key advantage of using the ONC cable array and linked communication system is that it extends seaward sufficient to test instrumentation at vent sites associated with the well-studied Endeavour Segment of the Juan de Fuca Ridge.

The vent site chosen for sampler deployment, the Main Endeavour Field-South science node study site, is in the immediate vicinity of the

S&M vent (Fig. 1), which has been visited and sampled using conventional approaches numerous times over more than thirty years (Butterfield et al., 1994). The chemistry of hydrothermal fluids issuing from vents associated with this site have also been sampled in 1999, 2005, and 2014 using similar conventional approaches by research teams from the University of Minnesota (Foustoukos et al., 2004, 2009; Seyfried et al., 2003). These more recent investigations were conducted to test the performance of in-situ redox and pH sensor systems (Ding and Seyfried, 2007; Ding et al., 2005). The on-line hydrothermal vent sampling system described here was deployed at the S&M vent area in September 2019 and recovered in June 2020, during which nine vent fluid samples were acquired remotely through the internet, all in the absence of seagoing assets.

2. Facilities, procedures and methods

2.1. Remotely operated serial sampler

The vent fluid sampler is designed as a manifold fluid acquisition system comprising twelve isobaric sampling chambers, each fitted with an independently operated, computer controlled, high-pressure valve (Fig. 2). A separate control unit houses electronics for valve operation, temperature measurement, data storage and communication (Fig. 2). All wetted components involved in sample acquisition and storage, and sampler control and communications are constructed of titanium or PEEK, effectively precluding corrosion in high-temperature hydrothermal fluid or ambient seawater. Upon establishing communication with the sampler, commands can be sent remotely to open and/or close motor-driven high-pressure valves directly connected to the isobaric cylinders in which the sampled vent fluid is acquired and retained. The isobaric design of each of the 12 sample chambers (160 ml) is similar in principal and functionality to that reported by others (Seewald et al., 2002; Wu et al., 2015), in that ocean bottom pressure is maintained as the sample inlet valve is triggered and vent fluid enters the sample chamber (Fig. 2). The sample cannister fills in response to differential pressure with respect to ambient conditions, such that fluid and gas components of the acquired sample are taken at seafloor pressure. This procedure prevents degassing, which would have implications for pH and the stability of many components in the sampled fluid. Lab tests indicate a fill rate of approximately 2 min at 20 MPa, roughly equivalent seafloor pressure at Main Endeavour Field. As initially described by Seewald et al. (2002), the fill rate is dictated by a combination of the pressure differential and the orifice size of an internal flow restrictor. To avoid entrainment of mineral deposit debris, a titanium mesh filter (size 0.5 mm pore size) is used to enclose the sampling inlet tubing of the snorkel (Fig. 2b). The multi-layered titanium mesh provided a more effective filtering mechanism beyond the base mesh size.

The mechanical and electrical components of the sampling system utilized here are similar in design to the "serial sampler" reported by Wu et al. (2015). It is important to emphasize, however, that the control valves used for the present system are commercially available high-pressure, titanium valves (High-pressure 2011LF4T15). Thus, the opening and closing force on the valve is actuated by the amperage imposed on the motor drive, which is pre-programmed in the electronics software, similar to valve-related operational control characteristics developed by Seewald et al. (2002). The snorkel serves as the primary inlet for vent fluid and is elongated to allow deeper penetration into the seafloor chimney structures (\sim 15 cm). A titanium sheathed thermocouple (Type K) attached to the sampling tubing of the snorkel permits temperature monitoring, which can be reported continuously owing to cable power permitting real-time two-way communication. This temperature monitoring capability is especially critical during the initial stages of sampler deployment as the snorkel can be precisely positioned in the region of optimal vent fluid temperature and flow rate. Away from the snorkel tip, titanium tubing is used to extend thermal tolerance of the sampler as the initially hot sampled fluid moves towards the containment cylinders when this is permitted to do so by valve operation. The titanium tubing, however, transitions to 0.125-inch OD $(0.062\,\mathrm{ID})$ PEEK tubing, which provides the flexibility necessary to correctly position the snorkel in the vent without needing to reposition the sampler as well. The internal volume of the PEEK and titanium tubing through which the vent fluid passes during normal sampling operations is approximately $10\,\mathrm{ml}$. This volume is initially filled with seawater, which occurs naturally during sampler transit by ROV to the seafloor.

The effective weight of the sampler in water is approximately 91 kg, which is offset significantly by syntactic foam secured to all sides of the unit (Fig. 4a and b). Lab tests have demonstrated effective operation of the sampling system at pressures as high as 70 MPa. While the core unit of the instrument (piston cylinders and supporting valve manifold) is highly temperature tolerant, electrical control units are not (Fig. 4a

right) and care must be taken during deployment to avoid exposure of the electrical system to discharging vent fluid.

2.2. Samper deployment on ONC

Ocean Networks Canada's NEPTUNE cabled observatory provides unique scientific and technical capabilities that enable scientists to deploy instruments on the seafloor via ONC junction boxes and to receive data remotely through network connections (Fig. 3). Deployment of the sampler at MEF in September 2019 was carried out by use of ROV *Odysseus* and CCGS *John P. Tully*. Owing to the considerable weight of the sampler (see above) and associated control systems (Fig. 4a), syntactic foam board was secured to all sides of the containment structure (Fig. 4b). The sampler was then positioned within a few meters of the desired vent structure in the S&M region of the MEF and powered

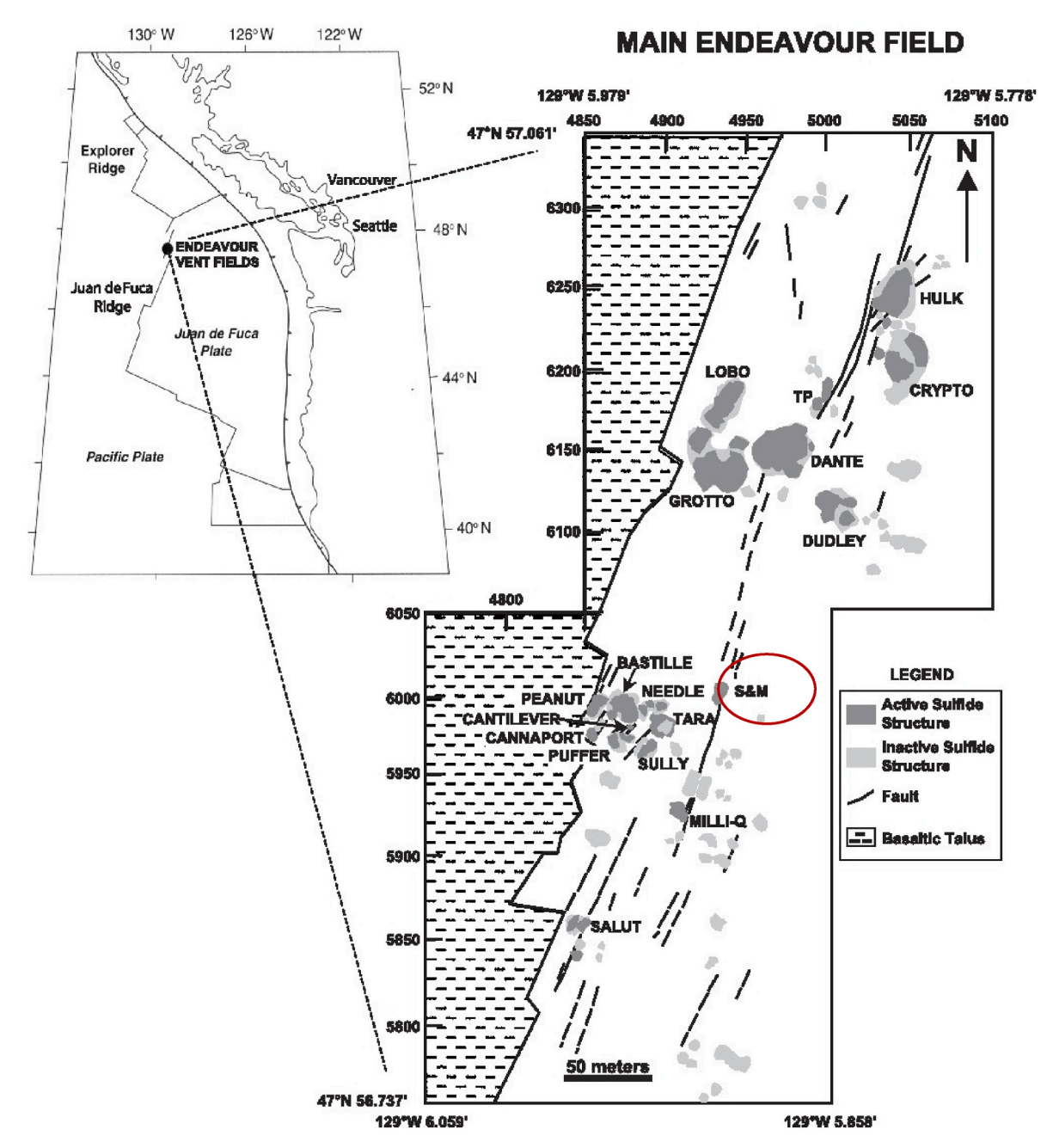


Fig. 1. Overview map showing location of the Main Endeavour Field relative to the Juan de Fuca Ridge, major regional plate boundaries, and coastlines. Small-scale geologic map of hydrothermal vents at Main Endeavour Field (MEF), northern Juan de Fuca Ridge. Red oval highlights the study site at/near S&M vent in the central/southern portion of MEF. MEF vent field map modified after Delaney et al. (1992), Seyfried et al. (2003), and Foustoukos et al. (2009).

by 48V DC power routed through ONC's Main Endeavour Field South Science junction box. The vent structure at which the sampler was deployed was occupied by a resistivity/temperature probe designed and built at the University of Washington by Dr. Marv Lilley and co-workers (Larson et al., 2007), which goes by the acronym, BARS (Fig. 4c). The BARS sensor had been reporting temperature and resistivity data at the vent site for at least a year prior to the sampler deployment. The size and shape of the vent orifice, however, accommodated the sampler snorkel without disturbing the BARS probe, as indicated by BARS temperature data collected during sampler installation. Just prior to departure of the ROV from the vent structure following sampler deployment, the sampler thermocouple recorded a steady state fluid temperature of 299 °C, while the BARS resistivity sensor reported a temperature of 302.5 °C.

2.3. Subsampling and analysis of hydrothermal vent fluids

An obvious advantage of the hydrothermal vent fluid sampler is that fluids issuing from seafloor chimney structures can be acquired remotely and on-demand in response to a pre-determined time schedule, as was often the case here, or to changes in physical factors, such as temperature or seismicity, if co-monitored. Samples acquired are maintained at pressure in their respective containment vessels for the entire duration of the deployment, until the sampler is recovered from the seafloor and the samples extracted in accordance with procedures developed over many years of hydrothermal vent research (Pester et al., 2011; Seewald et al., 2002; Seyfried et al., 2003). It has been long recognized that highly reactive components, such as dissolved Cu and other poorly soluble components (trace transition metals) tend to precipitate rapidly while contained within virtually all vent fluid samplers in response to temperature change, immediate processing notwithstanding. These "dregs" are subsequently rinsed from the sampler, collected by filtration, and ultimately dissolved in a mixture of HCl and HNO3 acids. Analyses of the acid digested metal-bearing products are then mathematically combined with those of residual metals in the coexisting dissolved fractions to effectively reconstruct vent fluid chemistry as it initially entered the sampler (Rouxel et al., 2008; Seewald et al., 2002). This same process was used in the course of the sampler deployment at S&M

vent area in 2019-2020.

Subsampling of the individual, pressurized sample containers was carried out at the University of Minnesota approximately two weeks after the return of the CCGS John P. Tully to port in Sidney, Canada (June 2020). As is the case with virtually all isobaric-type samplers, the initial step in fluid sample extraction involves valve connection of the back pressure fluid reservoir to a high-pressure pump and gauge. Upon first opening the valve, the pressure gauge should report the seafloor pressure at which the sample was obtained. All the individual sample chambers indicated 22 MPa pressure, broadly consistent with seafloor pressure at MEF, suggesting that the opening and closing of the respective inlet sample valves (vent fluid sampling) was successfully achieved. Extraction of the fluid contents of any sample chamber is enabled by pressurizing a series of pistons in the sampler, causing displacement of the sample fluid upon opening the sample inlet valve, in a manner consistent with that described in detail by Seewald et al. (2002).

Fluid samples incrementally extracted in this way were analyzed for pH, dissolved gases (CH₄, H₂, CO₂), dissolved H₂S, sulfate and other major and minor dissolved species. Detailed descriptions of analytical methods used in sample processing are included in previous studies of hydrothermal vent fluids conducted at the University of Minnesota (Foustoukos et al., 2009; Pester et al., 2011; Seyfried et al., 2015). Analyses of all major dissolved cations/anions were conducted using ICP-OES and/or ion chromatography, while minor and trace meals were determined by ICP-MS. Often, both instruments were used to better constrain the composition of the sampled fluids. As emphasized above, "dregs" fractions recovered from each of the sample cylinders were processed and analyzed in a manner generally consistent with typical vent fluid sampling protocols (Seyfried et al., 2003). The analytical uncertainties (1 σ) are estimated by replicate measurements to be: $\pm 2\%$ for major and minor dissolved cations and anions, although uncertainties in reported concentrations of these species increase with decreasing concentration, as is typical of limits imposed by the sensitivity of instruments (see above) used to make respective measurements (see above). Uncertainties of <10% for H₂S (iodometric titration) and <5% for CH₄ and H₂ (gas chromatography) were obtained, while

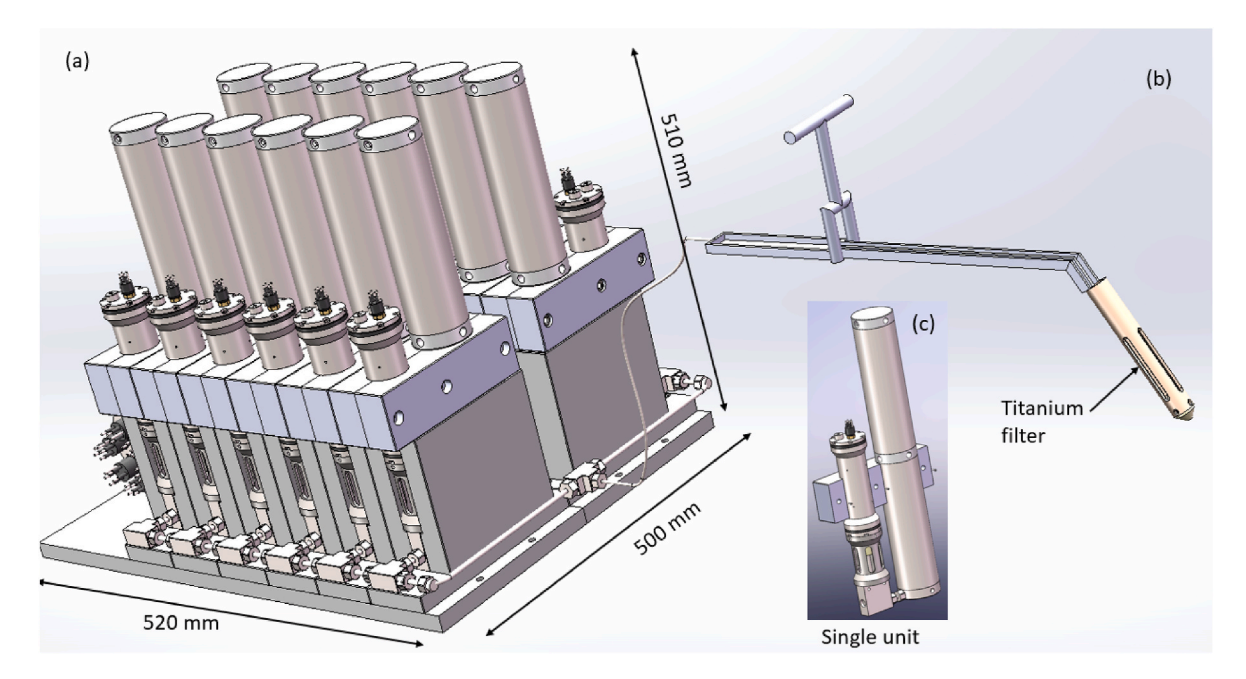


Fig. 2. A schematic 3D model of the hydrothermal vent fluid sampler that displays twelve independent core sampling units (a). Sampler snorkel (b) is elongated for deeper insertion into chimney orifice and fit with an external titanium filter to exclude solid debris more effectively. At the time of deployment, real-time temperature data allowed for optimal positioning of the snorkel in the high temperature vent fluid. Inset figure of a single core unit of the sampler shows fluid reservoir container and associated valve (c).

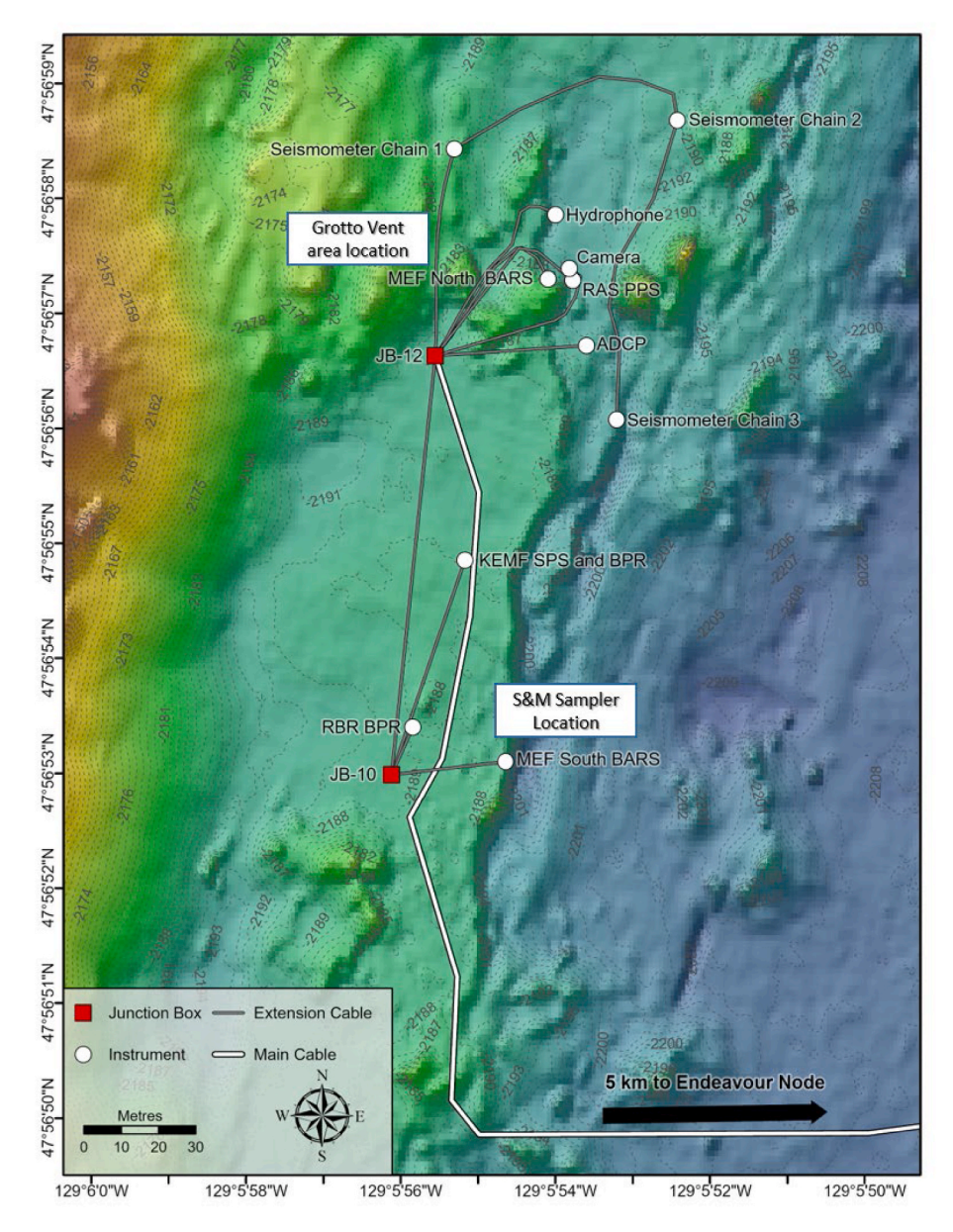


Fig. 3. Imagery of the coverage of ONC powered instrumentation at the NEPTUNE observatory, Main Endeavour Field. The location of seafloor cables and individual instruments or groups of instruments at vents are indicated. The S&M Sampler Location at which the hydrothermal vent fluid sampler was deployed and operated for nearly nine months is clearly indicated, along with the MEF South BARS resistivity probe that served as temperature backup.

uncertainties in reported concentrations (1 σ) are estimated by repeat measurements to be: $\pm 5\%$ for Mn, $\pm 5\%$ for Fe, and $\pm 10\%$ Ba.

3. Results and discussion

3.1. Near-seafloor compositional constraints: time series changes

The first fluid sample was taken approximately 1 month into the deployment on October 08, 2019 (Table 1). The sampling delay was performed to allow the vent/chimney system to recover from disturbances in fluid flow induced by positioning of sampler/snorkel in the vent orifice at the time of initial deployment. Internet communication was established with the sampler at the vent site through the ONC cable network and valve A1 (first fluid sample) was triggered from the University of Minnesota. This operation was repeated every 2–3 weeks for the first three samples, transitioning to near one-month intervals for the remainder of the deployment, for a total of nine vent fluid samples (Table 1, Fig. 5). As noted, the temperature measured at the time of the

initial deployment and for approximately two weeks thereafter was observed to be $\sim\!295\text{--}299\,^\circ\text{C}$. Unfortunately, shortly after this time period, the thermistor for the reference temperature for the sampler failed due to an uncertain cause, possibly related to localized heating by hydrothermal fluid escaping from the base of the chimney structure. The co-located ONC/UW BARS instrument, however, logged temperature continuously throughout the entire sampler deployment interval and, thus, provided an alternate means to obtain temperature data that could be accessed in near real time through ONC's online data portal and plotting utility (Owens et al., 2022). In general, the BARS temperature data indicate relative constancy through sample 6, although a noteworthy decrease in temperature from approximately 304 °C to 279–285 °C occurred abruptly, just prior to the last two months of the deployment and acquisition of last three vent fluid samples (Fig. 5).

3.1.1. Magnesium and sulfate

The quality of high-temperature hydrothermal vent fluids obtained by sampling at deep sea vents is typically evaluated with reference to

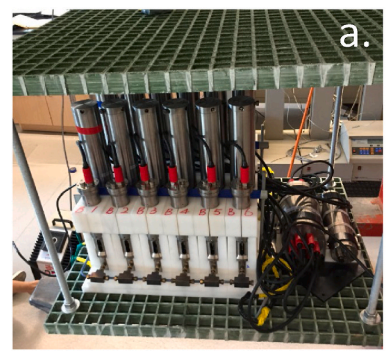






Fig. 4. Hydrothermal vent fluid sampler in the lab where an external framework was constructed around 12 sample canisters and computer control and communication systems (a). The effective weight of the sampler is \sim 200 kg in air and 91 kg when submerged in water. Syntactic foam for enhanced sub-sea buoyancy was added to the sampler for positioning on the seafloor at the targeted vent site (b). Sampler snorkel being inserted into the S&M vent orifice. Initial vent fluid temperature was reported to be 299 °C. The previously deployed and co-located BARS resistivity probe (see text) can be viewed in the chimney wall adjacent to the sampler snorkel. The BARS device and sampler snorkel occupy the same trunk of the chimney and thus are in close proximity (c). Sulfide chimney growth often encapsulates instrumentation in relatively short periods of time, effectively isolating the instrument in the path of the vent fluid.

Table 1 Chemical composition of 9 hydrothermal vent fluid samples remotely acquired during the \sim 9- month deployment at S&M vent, MEF (see Section 2.2). Concentrations are reported in mmol/kg (mm) or μ mol/kg (um). The dates at which the samples were obtained are indicted.

	Date		pH	Cl	H_2S	SO_4	Br	Na	K	Li	Mg	Ca
Sample	(MM/DD/YY)	Days	(25 °C)	mm	mm	mm	mm	mm	mm	um	mm	mm
1	10/08/19	0	4.21	424	2.71	0.12	0.75	330	21.5	380	0.24	30.9
2	11/01/19	24	4.29	443	3.25	0.09	0.81	349	22.8	410	0.19	33.1
3	11/20/19	43	4.22	453	2.83	1.05	0.82	400	25.1	432	2.55	35.3
4	12/12/19	65	4.49	437	3.61	0.71	0.78	337	21.0	365	2.35	30.1
5	01/15/20	99	4.27	451	3.37	1.40	0.82	368	22.7	392	3.07	32.3
6	02/28/20	143	4.06	432	3.24	0.63	0.77	350	22.0	392	1.39	31.9
7	03/19/20	163	4.22	428	3.12	0.21	0.77	347	21.5	388	0.80	31.5
8	04/17/20	192	4.37	432	3.49	0.23	0.77	349	21.2	404	0.63	32.4
9	05/26/20	231	4.13	429	3.40	0.23	0.75	332	22.7	396	0.56	31.8
Sample	Days	Ва	Fe		Mn	Sr	S	i	CH ₄	С	O ₂	H_2
		um	um		um	um	n	nm	mm	m	ım	mm
1	0	50	281		236	113	1	4.1	1.71	7.	.21	0.23
2	24	64	385		251	121	1	5.2	1.88	7.	.31	0.24
3	43	22	441		262	128	1	6.4	1.80	7.	.48	0.23
4	65	43	284		221	108	1	3.3	1.73	7.	.06	0.22
5	99	8.1	777		240	116	1	4.7	1.76	7.	.67	0.20
6	143	23	387		239	115	1	5.1	1.52	5	.94	0.21
7	163	40	189		237	114	1	4.8	1.54	6	.16	0.21
8	192	37	214		243	118	1	4.8	1.82	5	.87	0.24
9	231	35	176		235	116	1	5.4	1.75	7.	.21	0.23

dissolved Mg concentrations, with low Mg concentrations indicating higher-quality samples. Experimental and theoretical data have confirmed that the hydrothermal fluid endmember would have only trace concentrations of dissolved Mg (Janecky and Seyfried, 1984; Seyfried and Bischoff, 1981) owing to constraints imposed by the relative insolubility of Mg-bearing minerals at elevated temperatures. Seawater, in comparison, contains 53 mmol/kg Mg. Thus, even small amounts of seawater mixing with a hydrothermal fluid can be detected based on the relative abundance of dissolved Mg. To account for seawater mixing effects, the composition of a hydrothermal fluid component is typically extrapolated to zero Mg to calculate the so-called hydrothermal "endmember" vent fluid (Butterfield et al., 1990, 1994; Seyfried et al., 2003; Von Damm et al., 1985). Using this metric, the Mg concentrations of 0.2-3.1 mmol/kg in the remotely obtained samples show that they are overwhelmingly dominated by the hydrothermal component (Table 1, Fig. 6).

Like Mg, dissolved sulfate is typically depleted relative to seawater in endmember hydrothermal vent fluids. This results from the retrograde solubility of anhydrite during seawater circulation in the ocean crust (Bischoff and Seyfried, 1978; Seyfried and Bischoff, 1981), but also

because high temperature hydrothermal source conditions are typically basalt dominated and moderately to distinctly reducing. Both conditions can be expected to decrease dissolved sulfate and increase dissolved H2S with reaction progress and increasing temperature. Notably, the first two samples contain Mg and sulfate concentrations of 0.24 and 0.19 and 0.12 and 0.09 mmol/kg respectively, which is comparable to the range of apparent equilibrium Mg and sulfate concentrations reported by Seyfried and Bischoff (1981) for basalt-seawater alteration at 300 °C, 500 bar (Mg = 0.04 mmol/kg, sulfate = 0.2 mmol/kg). In terms of mid-ocean ridge vent fluids, these are some of the lowest concentrations of Mg and sulfate yet reported and may for the first time provide insight into more deeply seated hydrothermal alteration processes. It is important to note that our ability to retrieve these apparently uncompromised Mg and sulfate data in the first two samples is surprising, as the sampler snorkel and dead volume in general had to contain seawater at the time of initial deployment at the vent owing to infiltration on descent to the seafloor. The lack of chemical evidence for seawater-filled dead volume, however, is almost certainly the result of the nearly one-month hiatus between the time of initial deployment and acquisition of the first sample. The intervening time was apparently sufficient

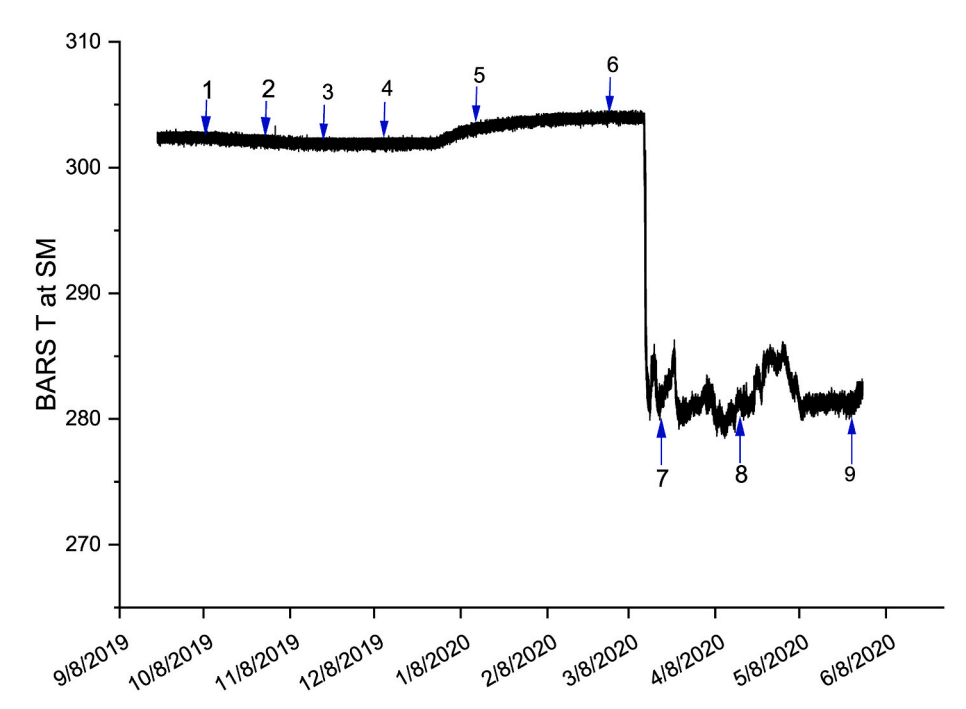


Fig. 5. Real-time temperature record from a BARS probe in the S&M vent together with the sampler snorkel (see Section 2.2). The BARS probe provided insight on changes in the vent fluid temperature throughout the ~9-month deployment interval. Although there is little change in temperature for early-to intermediate time samples (1–6), this is not the case for the last three samples (7–9), where temperature decreases by approximately 20 °C, with corresponding changes in highly temperature sensitive transition metals, such as Fe, Cu and Zn (see text).

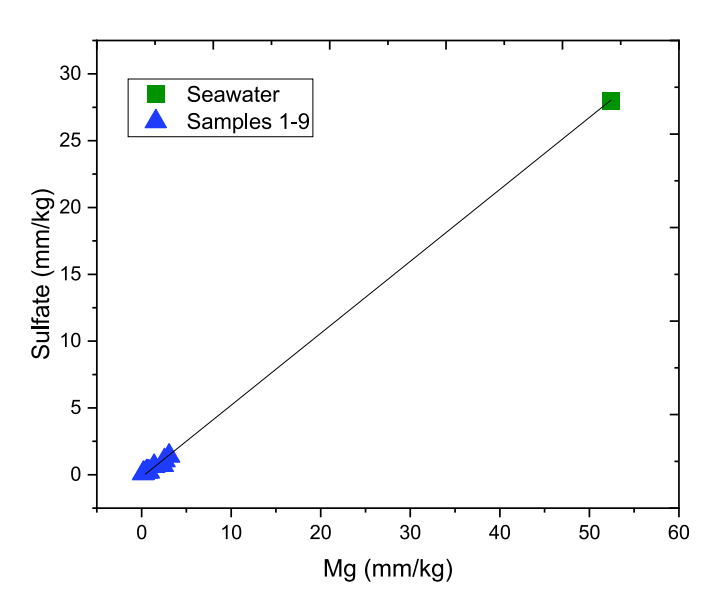


Fig. 6. Dissolved sulfate and Mg concentrations in remotely obtained vent fluid samples. These data generally indicate high quality of the sampling as shown by the exceedingly low sulfate and Mg in the samples, especially for early and late samples (see text and Fig. 7). In effect, the values reported here are the lowest yet measured for seafloor hydrothermal vent fluids, with implications for subseafloor hydrothermal alteration processes.

for seawater contained in the snorkel to mix and exchange completely with vent fluid, thereby providing an effective means to acquire a vent fluid sample uncompromised by seawater chemistry. Such a lengthy delay in sampling would not be possible under the limited time constraints associated with conventional sampling techniques.

Although there is no question that both sulfate and Mg are greatly depleted in the sampled vent fluids relative to seawater (Table 1, Fig. 6), closer examination of these data reveals a finer scale covariation in Mg and sulfate, suggesting ingress of a Mg- and sulfate-bearing fluid that abruptly commenced at about the time of the third sample, approximately 43 days into the deployment (Table 1, Fig. 7). Although ambient seawater was a first consideration, this sample and all subsequent

samples reveal sulfate/Mg ratios that depart significantly from that of seawater (Fig. 7). Interestingly, the incursion event is particularly obvious in samples 3–5, 43–99 days into the deployment, before gradually subsiding, as both dissolved sulfate and Mg concentrations decrease together and trend toward the distinctly low concentration conditions characteristic of the earliest samples acquired (Fig. 7). Accordingly, at the time of sampler recovery (05/26/20, ~231 days of operation), the first and the last fluids acquired reveal largely similar Mg and sulfate concentrations, and in both cases are overwhelmingly dominated by the hydrothermal endmember, likely sourced deep in the ocean crust from which the vent fluid is largely derived. The ultimate

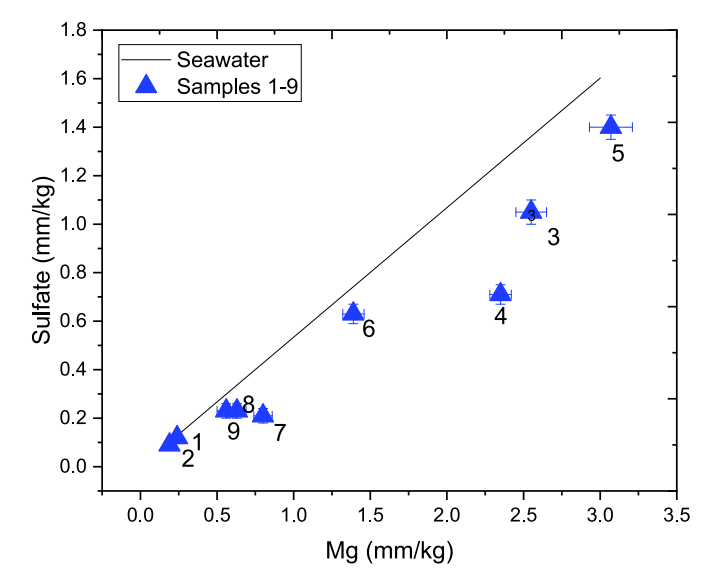


Fig. 7. Time series change in dissolved Mg and sulfate concentrations in fluid samples in comparison with a seawater tend line. These data show: a) Unusually low Mg and sulfate concentrations in samples 1–2; b) incursion of compositionally modified seawater (samples 3–6) with a sulfate/Mg ratio lower than seawater; and c) return to low Mg and sulfate concentrations (7–9) with values broadly similar to the early samples (see text). These data underscore the utility of time series sampling at a single vent to assess the dynamics of near surface reaction path processes.

cause of the incursion, however, is unclear and may relate to changes in permeability in the immediate subsurface of the chimney/vent environment caused by mineral dissolution/precipitation processes and/or localized seismicity.

If the anomalous Mg and sulfate bearing fluid is not ambient seawater (Fig. 7), an alternative interpretation might include conductively heated seawater. A hypothesis such as this might result in anhydrite precipitation and related cation exchange reactions with the potential to modify seawater chemistry, especially involving reactive components such as sulfate and Mg. Indeed, previous basalt-seawater experiments conducted at 70 °C (Seyfried and Bischoff, 1979), 125 °C (Brant et al., 2012), 150 °C (Seyfried and Bischoff, 1979), 200 °C (Bischoff and Dickson, 1975), and 300 °C (Seyfried and Bischoff, 1981) suggest that sulfate/Mg ratios less than seawater are broadly indicative of seawater/rock reactions at temperatures >150 °C. It is important to note, however, that all but the lowest temperature experiments trend towards a reaction stage at which Mg and sulfate are depleted below what is observed in the most Mg-rich MEF fluid sample (Mg = 3.07 mmol/kg) and/or that sulfate/Mg ratios ultimately evolve to greater-than-seawater values. While experimental results and reaction times should be applied only cautiously to natural systems, it is reasonable to conclude that a combination of temperature and time for basalt-seawater reaction can produce fluids broadly analogous to the anomalous Mg and sulfate bearing fluids recognized for the MEF samples at the intermediate stages of chemical evolution.

3.1.2. Temperature and dissolved iron

The BARS temperature record must be viewed cautiously when applying these data to interpret the cause of changes in fluid chemistry in the acquired time series samples at MEF. For example, the influx of anomalous Mg-sulfate fluid elicited no apparent temperature response from BARS. In this case, however, the small amount of fluid entrained (~3%), as well as the likelihood that temperature of entrained fluid exceeded that of ambient seawater, may have played a role in this. On the other hand, the mechanism, source, and amount of fluid and how and where it enters the chimney structure relative to the position of the BARS probe and sampler fluid inlet can undoubtedly affect the relationship between chemical and thermal signals. Thus, in some cases, because of a coalescence of physical factors, the correspondence between the BARS probe and chemical changes in the sampled vent fluid may be more meaningful. Such may be the case late in the deployment. For example, approximately two weeks after sample 6, ONC (BARS) archival data indicate that vent fluid temperatures abruptly decreased from 302-304 °C to 281-282 °C (Fig. 5). This temperature change had no significant effect on major dissolved species (Table 1). This indicates little or no change in the composition or conditions at the fluid source at depth in the ocean crust. However, Fe concentrations in samples collected after this temperature change (samples 7-9) are significantly lower than the average of all samples prior to this event, with similarly noteworthy decreases in the Fe/H₂S ratio. Preliminary data for other transition metals, such as Cu and Zn, reveal much larger decreases in concentration relative to Fe subsequent to this late-stage cooling event. The temperature dependent solubility of these metals is well known (Seewald and Seyfried, 1990). Thus, the observed changes are not surprising, and provide strong evidence that the BARS temperature data reflect a real decrease in vent fluid temperature, an interpretation that works against the notion that the BARS probe and sampler inlet are not effectively co-located.

Although there is much to learn about the processes responsible for the time, temperature, and composition correlations recognized from the sampler deployment, what is clear is that in the absence of the time series data, the questions with which we are now concerned could not have been foreseen, underscoring the combined value of cable power, continuous data acquisition and delivery and on-demand remote sampling capabilities.

3.1.3. Barium

The low dissolved sulfate that characterizes sampled vent fluid composition, both early and late in the deployment, effectively serves as a means to evaluate time series changes of other components that are known to be sensitive to the dissolved concentration of sulfate in the coexisting fluid. Chief among these is dissolved Ba. Owing to the low solubility of barite in sulfate bearing fluids (Hanor, 2000; Jamieson et al., 2016; Monnin, 1999; Monnin et al., 2003; Shikazono, 1994) and the extent of seawater mixing that often characterizes vent fluid samples, estimation of the endmember Ba concentration from midocean ridge hydrothermal sources has been difficult. This has required application of novel approaches based on Ba isotope fractionation models to achieve more robust estimates (Hsieh et al., 2021). It can, however, be inferred that dissolved Ba concentrations in the first two acquired samples (Table 1), with concentrations of approximately 50 and 64 µmol/kg respectively, provide good indicators of true endmember Ba concentrations in vent fluids at MEF. The low dissolved sulfate in these samples clearly plays a role in this. Furthermore, this view is reinforced by the closeness of these values to the Ba isotope-based estimate of 70 \pm 6 µmol/kg produced for Bastille vent fluid, another MEF vent very near the S&M structures (Fig. 1) (Hsieh et al., 2021). As is the case here and at nearby Bastille vent (MEF), mass balance calculations indicate that about 50-70% of the total dissolved Ba precipitates in the sampler, as part of the dregs fraction, presumably as barite. With the onset of sulfate incursion, as described above, total Ba concentrations in sampled vent fluid (including dregs fractions) also decrease, as might be expected with barite precipitation in the seafloor. A reversal of this behavior is observed after the sample retrieved on 01/15/20 (sample 5), signaling diminished input of sulfate (Figs. 7 and 8) and correspondingly higher levels of dissolved Ba. That the total Ba (fluid plus dregs) is not conservative over the full course of the deployment, suggests that some Ba (barite) may be lost to the chimney environment during or after mixing with reacted and heated seawater. Notably, the presence of barite has been recognized in precisely these deposits (Gartman et al., 2019). There can be no question that the coming and going of the addition of relatively small amounts of sulfate from a still uncertain source to the

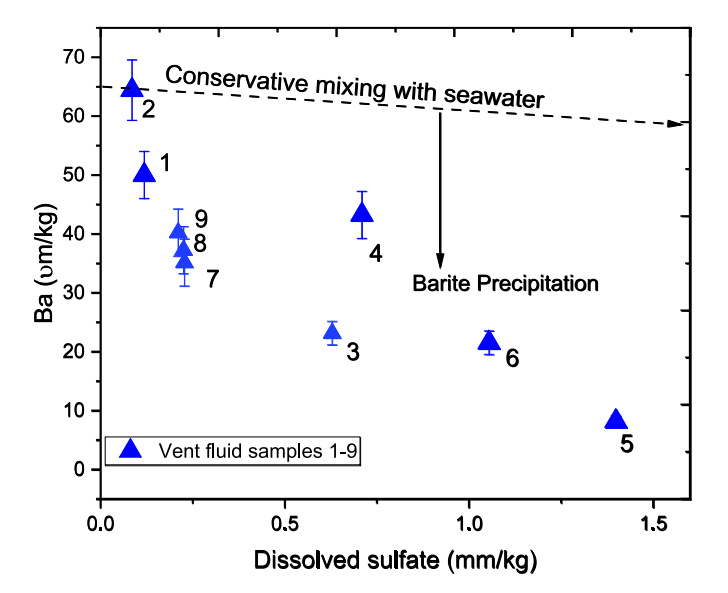


Fig. 8. Dissolved Ba and sulfate concentrations in vent fluid samples throughout the approximately 9-month deployment. The decrease in dissolved Ba with increasing sulfate (samples 1–5, see Table 1) suggests barite precipitation. Subsequent samples (6–9, Table 1) show Ba increase as sulfate incursion decreases. As noted previously, the source of sulfate (and Mg, see Table 1) is inferred to be conductively heated and partially altered seawater (see Section 3.1.1). The decrease and increase in Ba concentration during the deployment is significant and underscores process-oriented insights obtainable from time series samples at a single vent.

hydrothermal up flow zone has a dramatic effect on Ba solubility in the sampled high-temperature vent fluid, once again revealing a process completely unanticipated from all previous vent fluid sampling efforts using conventional approaches. However, the uncertain chemical and physical parameters (temperature, fluid-rock mass ratio, rock, mineral, and fluid Ba concentrations) of the "secondary" source fluid that provides the anomalous Mg and sulfate concentrations that so clearly influence the flux of Ba from the sampled vent fluid make it difficult to model unambiguously the reaction path processes and phase equilibria central to the controls on Ba solubility in the dynamic vent/chimney system (Fig. 8).

3.2. Subseafloor pressure-temperature conditions

As is typical of hydrothermal fluids in the southern region of the Main Endeavour Field (Fig. 1), the sampler data (Table 1; Fig. 9) confirm the vapor-rich nature of the source fluid (approximately 20% below seawater salinity). This observation indicates that these fluids are derived at relatively high temperatures and pressures, displaced slightly from the critical curve in the two-phase NaCl-H₂O system (Bischoff and Pitzer, 1989; Bischoff and Rosenbauer, 1987; Coumou et al., 2009; Driesner and Heinrich, 2007; Foustoukos and Seyfried, 2007; Scott et al., 2017)

Although phase separation clearly influenced vent fluids obtained at the S&M vent area during the 2019-2020 sampler deployment on the ONC network, it would appear from the modest depletion in dissolved Cl relative to seawater that the pressure-temperature conditions in the subsurface from which the fluids are derived must be well in excess of analogous conditions at the seafloor. To assess this we apply the Si-Cl based geothermobarometer developed by Fontaine et al. (2009). This method takes advantage of the pressure-temperature dependent solubility of both quartz and Cl in the two-phase region of the NaCl-H₂O system. At a given pressure-temperature condition within the vapor-liquid region of the NaCl-H2O system, the NaCl content, and therefore density, of both the vapor and liquid are invariant (Liebscher and Heinrich, 2007). Unique subsurface conditions can then be calculated using measured concentrations of $SiO_{2(a_{\text{q}})}$ and Cl in vent fluid samples. In addition to the presence of quartz, the Si-Cl method assumes that SiO_{2(aq)} and Cl concentrations equilibrate during phase separation

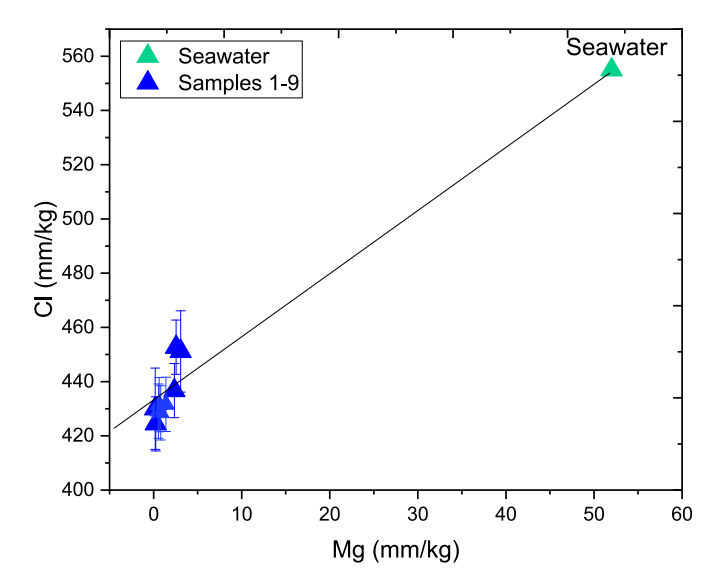


Fig. 9. Dissolved Cl and Mg concentrations in fluid samples illustrating the successful acquisition of the hydrothermal endmember, as indicated by exceeding low Mg concentration, and generally stable Cl concentrations. The "endmember" chloride concentration indicates a vapor phase source fluid in good agreement with previous studies of the hydrothermal vent fluid chemistry at MEF over many years (see text).

and remain constant during ascent to the seafloor. This assumption is likely justified as even a small amount of conductive cooling would place the vapor in the one-phase region of the NaCl-H₂O system, effectively precluding further separation of Cl-bearing components from the compositionally homogeneous fluid. Using this relationship as initially proposed by Fontaine et al. (2009) suggests a temperature and pressure of approximately 435 °C and 38 MPa. More recently, Scheuermann et al. (2018) conducted quartz solubility experiments in the two-phase NaCl-H $_2$ O system from 420 to 500 $^{\circ}$ C and pressure from 31 to 52 MPa. These data benefitted from revised correlation algorithms for density and other fluid transport properties in temperature-pressure-composition space from 0 to 1000 °C, 0-5000 bar, and 0 to 1 X_{NaCl} (Driesner and Heinrich, 2007). Importantly, the experiments and revised density data permitted calibration of prominent density-based quartz solubility models (Akinfiev and Diamond, 2009; Fournier, 1983; Von Damm et al., 1991), optimizing application and testing of these models for marine hydrothermal systems, where vapor-liquid coexistence in the NaCl-H₂O system is widespread. When applied to the average chloride and silica concentrations from the ONC sampler data (Table 1), temperature-pressure conditions of 490 °C and 48 MPa are indicated. In comparison with constraints imposed by the seismically imaged axial magma chamber underlying the Main Endeavour Hydrothermal Field, the recent quartz-Cl solubility data would suggest depths of hydrothermal circulation broadly consistent with the putative location of AMC (Arnoux et al., 2017; Van Ark et al., 2007).

Other components in the vent fluids acquired at S&M vent with the remotely operated sampler provide evidence linking these fluids to characteristics long recognized for the MEF system. Although not a quantitative indicator of the quality of hydrothermal fluid samples from MEF vents, the relatively high dissolved methane concentrations reported here (Table 1) are in keeping with a well-known feature of these fluids (Lilley et al., 1993, 2003; Seewald et al., 2003). Based on light carbon isotope signatures and association with anomalously high ammonium concentrations, it has been previously proposed that the methane is a product of thermogenic decomposition of organic matter, possibly linked to seawater recharge and reaction with buried turbiditic sediments (Lilley et al., 1993). Moreover, from an assessment of systematic variations in the correlation of alkali metals and B as a function of Cl concentration, Butterfield et al. (1994) concluded that interaction with sediment was occurring prior to phase separation. This interpretation is consistent with recent clumped isotope data for methane, which place the methane formation temperature at approximately 360 °C (Douglas et al., 2017). On the other hand, the combination of steady state redox (H2 and H2S) and pH data (Table 1) indicate phase equilibria controls and highly rock-dominated alteration conditions in the source fluid region at depth that ultimately provide compositionally evolved fluids that issue from the S&M vent area and likely neighboring vents in the Main Endeavor Field (see Section 3.3). These inferences are based on the generally good agreement between the vent fluid data and constraints imposed from lab experiments at broadly analogous chemical and physical conditions (Ding and Seyfried, 1992, 1995, 1996; Seyfried and Ding, 1995). The relatively high concentrations of K, Li, and Sr, all good indicators of the integrated fluid/rock mass ratio (Berndt and Seyfried Jr, 1990; Berndt and Seyfried, 1993; Berndt et al., 1989; Foustoukos et al., 2004), on an absolute or chloride normalized basis, support this conclusion (Table 1).

3.3. Time series observations of vent fluids at the S&M vent area: 1988–2020

The Main Endeavour Field (MEF) has been studied for more than three decades and the linkage between magmatic and tectonic events and hydrothermal processes has been well established (Butterfield et al., 1994; Chadwick and Embley, 1994; Delaney et al., 1992). The most complete examination of the time series changes of vent fluids at the

MEF is that of Butterfield et al. (1994). These investigators reported the chemistry of vent fluid samples from Endeavour collected in 1984, 1987 and 1988. In general, it was recognized from this study that each vent fluid had a distinctive chemistry, which remained relatively constant from one year to the next. However, a large compositional gradient was reported across the vent field, with end-member chloride concentrations increasing from about 100 mmol/kg in the southwest (Lilley et al., 1993) to 505 mmol/kg toward the northeast (Butterfield et al., 1994).

Hydrothermal fluids issuing from the S&M vent area have also been sampled by researchers from the University of Minnesota (UM) in connection with development and testing of chemical sensors for monitoring redox and pH of seafloor vent fluids. Subsequent analysis of S&M vent fluid chemistry shows a high degree of consistency of most chemical components throughout the sampled interval from 2005 to 2020 (Table 2). The sampler data reported in Table 2 (2019) represents the second sample of the time series study (Table 1) and is distinguished by its unusually low dissolved Mg concentration.

Dissolved chloride concentrations in fluids throughout the reported interval for the UM sample series show a slight decrease with time, but all samples reveal phase separation effects at conditions not far removed from the critical curve, as described in some detail earlier for the 2019 sample. Taken together with the similarly decreasing concentrations of dissolved silica, the data suggest that the earlier samples (2005, 2014) may have attained temperatures and pressures in excess of the values reported for the present study. Similarly, the relative constancy of dissolved Ca and Na implicates control by plagioclase of intermediate composition for the entire sample sequence, while potassium and lithium concentrations suggest alteration under generally rockdominated conditions throughout the reported time series (Berndt and Seyfried, 1993; Berndt et al., 1989; Foustoukos et al., 2004; Pester et al., 2012, 2015). Dissolved Fe is lower by about half in the 2019 sample in comparison with the earlier samples (Table 2), but other samples from 2019 have higher Fe concentrations, especially prior to the late-stage cooling event, in better agreement with the historical trend (Tables 1 and 2). Not surprisingly, Mn is in excellent agreement with all the historical data from the S&M vent (Table 2). Somewhat greater time series variability exists for dissolved H2, CO2, and CH4 (Table 2), but the concentrations of these species are still within the range of vent fluid compositions long reported for the MEF (Lilley et al., 1993, 2003). Dissolved H₂ is almost certainly controlled by a moderately oxidizing alteration assemblage, which, like plagioclase alteration, seems well buffered, providing yet a further indicator of the chemical and physical stability of the subseafloor hydrothermal system at MEF (Ding et al., 2001; Seyfried and Ding, 1995). This degree of stability is also consistent with the relative constancy of H₂S, pH and temperature reported for the S&M vent fluids for the approximately 15-year monitoring interval (Table 2). On a finer scale, however, S&M and other vents in the MEF can be affected by local seismic events and other still poorly understood phenomena that can result in small to moderate changes in seawater mixing and cooling with collateral effects on trace metal and dissolved gas concentrations. The important benefit of the remote operation and long-term deployment at an individual vent enabled by the newly developed vent fluid sampler is that these sorts of changes in near-field chemical and physical factors on the transport and deposition of trace and in some cases major elements can be quantitatively assessed. That samples can be obtained on demand and potentially in response to timely and accessible data on vent fluid temperature and seismic activity and on a temporal scale unachievable by conventional vent fluid sampling approaches provides added justification for deployment of the autonomous sampling system at other seafloor vent systems where broad scale compositional and physical variability can be explored.

4. Conclusions

A newly developed serial isobaric sampler was deployed by ROV at/near the S&M vent area of Main Endeavour Field, Juan de Fuca Ridge. The operational characteristics of the sampler take full advantage of the power and communication capabilities intrinsic to Ocean Networks Canada's NEPTUNE Observatory. Over the approximately 9-month deployment (September 2019 through May 2020), nine high-temperature fluid samples were acquired remotely over the internet from shore-based labs at the University of Minnesota.

Vent fluid chemical and temperature data from the remotely acquired samples provide insight on the temporal evolution of the S&M vent system and coexisting mineralization and heat and mass transfer processes. The first samples acquired indicate a temperature of approximately 299 °C that agrees well with temperatures reported by a co-located BARS sensor. Dissolved Mg and sulfate concentrations in these samples are exceedingly low, in keeping with experimental constraints on the concentration of these species in fluids coexisting with basalt and its alteration products at elevated temperature and pressures. Accordingly, these data provide previously unavailable insight on the solubility of both elements coexisting with greenschist or amphibolite bearing alteration assemblages at temperature and pressures considerably higher than seafloor vent conditions. The implications of this observation are particularly significant for testing models of redox and pH controls at depth in the ocean crust (Seyfried and Ding, 1995). Three subsequent samples, however, generally reveal slight but significant increases in the concentrations of Mg and sulfate, with a distinct sulfate/Mg ratio, likely attributable to incursion of conductively heated and partially reacted seawater. Although presently unresolved, the anomalous Mg and sulfate bearing fluid may have been entrained beneath the chimney structure, where localized heating effects are likely. The addition of even the modest amounts of sulfate that mixed with the primary source fluid during this interval caused a dramatic decrease in dissolved Ba, presumably as barite, which is consistent with constraints from recent models based on Ba isotopic systematics in venting seafloor hydrothermal fluids (Hsieh et al., 2021). The barite formation process is reversed in later samples, as indicated by noteworthy increases in dissolved Ba with decreasing sulfate and Mg, a phenomenon that has not

Table 2
Temporal variability of endmember vent fluid at/near the S&M vent site, MEF, from 2005 to 2019 (present study). As summarized in the text, the relative stability of chloride vapor-rich fluid, silica, and most other major dissolved species suggest subseafloor alteration and mass transfer buffered by reaction at elevated temperatures and pressures (~480 °C, ~48 MPa). Trace alkali element concentrations confirm rock-dominated conditions, as might be inferred from the high temperatures and constraints imposed by phase equilibria calculations (see text). Clearly, conductive cooling and decompression of the hydrothermal source fluids on ascent to the seafloor is a widespread process for MEF vents, a point raised by numerous investigators.

Year	Temp (°C)	Cl (mm)	pH 25 °C)	Ca (mm)	K (mm)	Na mm	Li (μm)	Fe (µm)	Mn (µm)
2019	303	443	4.29	33.1	22.8	349	410	385	251
2014	291	477	4.27	32.0	21.5	330	375	710	260
2005	314	484	4.40	36.0	23.8	392	295	750	239
Year	I	H ₂ S (mm)	Si (mı	m)	H ₂ (mm)		CO ₂ (mm)		CH ₄ (mm)
Year 2019		H ₂ S (mm) 3.25	Si (mr 14.9	m)	H ₂ (mm)		CO ₂ (mm) 7.31		CH ₄ (mm)
	3			m)					

before been measured at deep sea vents. These data provide an illustration of the dynamic nature of the hydrothermal vent environment, while underscoring the value of time series sampling at a fixed vent location on the seafloor. An abrupt temperature decrease of approximately 20 °C was reported by the BARS temperature sensor, shortly after acquisition of sample 6 (02/28/20). The temperature decrease was associated with a corresponding decrease in dissolved Fe (and other transition metals), providing evidence of the BARS probe as a reliable indicator of vent fluid temperature. These data provide further evidence of the changes in chemical and physical processes at deep sea vents that can occur on short time scales. In the absence of the time series sampling capability, the observed incursion of Mg and sulfate and later vent fluid cooling effects would not have been recognized. For the most part, however, most components recovered from the sampler provide insight on chemical and physical conditions in the source region from which the S&M vent fluid is ultimately derived. These data confirm long suspected phase equilibria controls, phase separation effects, and rock dominated mass transfer processes. In combination with conventional sampling of S&M vent fluids in 2005 and 2014, the present dataset underscores the remarkable stability of rock-buffered major element components in vent fluids in this area of the Endeavour Segment of the Juan de Fuca Ridge. Time series data described in this report are unique and highly insightful to a potentially wide range of vent related processes. When deployed in combination with other supporting instrumentation and ocean bottom seismometers, the remotely operated and on-demand sampling capability emphasized in this report can be used to constrain a wide range of time critical geochemical and biological processes. On a more practical level, that sampler deployment and operation overlapped in time with the early stages of the COVID-19 crisis, where seagoing operations in Canada and the U.S. were delayed or canceled, provides yet another example of the importance of the availability of remote sampling capabilities in ways that clearly could not be anticipated.

Declaration of competing interest

The authors declare that they have no known competing financial interests or personal relationships that could have appeared to influence the work reported in this paper.

Acknowledgements

The authors wish to thank Jeb Dexter and his colleagues at Ocean Networks Canada for helpful and constructive advice throughout the instrument development and testing interval. We would also like to thank the crew and pilots of ROV Odysseus and CCGS John P. Tully for their efforts during deployment and recovery of the instrument and Ocean Networks Canada for building and maintaining the cabled observatory that facilitated this research. Funding for the project was provided by the Canadian Foundation for Innovation (Project 30867), the U.S. National Science Foundation (EAR 1515377 and OCE 1736679) (WES), the National Natural Science Foundation of China (Grant No. 51879232) (SW) and the NASA Astrobiology Program ICAR Grant [80NSSC21K0592] Title: What life wants: Exploring the natural selection of elements" to Betül Kaçar (PI), WES and GNE. The authors also wish to thank Dr. D. I. Foustoukos and an anonymous reviewer for their thoughtful comments and suggestions that greatly improved the manuscript.

References

- Akinfiev, N.N., Diamond, L.W., 2009. A simple predictive model of quartz solubility in water–salt–CO2 systems at temperatures up to 1000°C and pressures up to 1000MPa. Geochem. Cosmochim. Acta 73 (6), 1597–1608.
- Arnoux, G.M., Toomey, D.R., Hooft, E.E.E., Wilcock, W.S.D., Morgan, J., Warner, M., VanderBeek, B.P., 2017. Seismic evidence that black smoker heat flux is influenced by localized magma replenishment and associated increases in crustal permeability. Geophys. Res. Lett. 44 (4), 1687–1695.

- Berndt, M.E., Seyfried Jr., W.E., 1990. Boron, bromine, and other trace elements as clues to the fate of chlorine in mid-ocean ridge vent fluids. Geochem. Cosmochim. Acta 54 (8), 2235–2245.
- Berndt, M.E., Seyfried, W.E., 1993. Calcium and sodium exchange during hydrothermal alteration of calcic plagioclase at 400°C and 400 bars. Geochem. Cosmochim. Acta 57 (18), 4445–4451.
- Berndt, M.E., Seyfried Jr., W.E., Janecky, D.R., 1989. Plagioclase and epidote buffering of cation ratios in mid-ocean ridge hydrothermal fluids; experimental results in and near the supercritical region. Geochem. Cosmochim. Acta 53 (9), 2283–2300.
- Bischoff, J.L., Dickson, F.W., 1975. Sea water-basalt interaction at 200 C and 500 bars. Implications for origin of sea-floor heavy-metal deposits and regulation of sea water chemistry. Earth Planet Sci. Lett. 25 (3), 385–397.
- Bischoff, J.L., Pitzer, K.S., 1989. Liquid-vapor relations for the system NaCl-H₂O: summary of the P-T-x surface from 300° C to 500° C. Am. J. Sci. 289, 217–248.
- Bischoff, J.L., Rosenbauer, R.J., 1987. Phase separation in seafloor geothermal systems: an experimental study on the effects of metal transport. Am. J. Sci. 287, 953–978.
- Bischoff, J.L., Seyfried Jr., W.E., 1978. Hydrothermal chemistry of seawater from 25 to 350 degrees C. Am. J. Sci. 278 (6), 838–860.
- Brant, C., Coogan, L.A., Gillis, K.M., Seyfried Jr., W.E., Pester, N.J., Spence, J., 2012.
 Lithium and Li-isotopes in young altered upper oceanic crust from the East Pacific
 Rise: insight into axial hydrothermal systems. Geochem. Cosmochim. Acta (in-press).
- Butterfield, D., Massoth, G., McDuff, R., Lupton, J., Lilley, M., 1990. Geochemistry of hydrothermal fluids from axial seamount hydrothermal emissions study vent field. Juan de Fuca ridge: subseafloor boiling and subsequent fluid-rock interaction. J. Geophys. Res. Solid. 95 (B8), 12895–12921.
- Butterfield, D.A., McDuff, R.E., Mottl, M.J., Lilley, M.D., Lupton, J.E., Massoth, G.J., 1994. Gradients in the composition of hydrothermal fluids from the Endeavour segment vent field: phase separation and brine loss. J. Geophys. Res. Solid Earth 99 (B5), 9561–9583.
- Chadwick, W.W., Embley, R.W., 1994. Lava flows from a mid-1980s submarine eruption on the Cleft segment, Juan de Fuca Ridge. J. Geophys. Res. Solid Earth 99 (B3), 4761–4776.
- Chave, A.D., Waterworth, G., Maffei, A.R., Massion, G., 2004. Cabled ocean observatory systems. Mar. Technol. Soc. J. 38 (2), 30–43.
- Chen, Y., Yang, C., Li, D., Jin, B., Chen, Y., 2012. Design and application of a junction box for cabled ocean observatories. Mar. Technol. Soc. J. 46 (3), 50–63.
- Coogan, L.A., Seyfried Jr., W.E., Pester, N.J., 2019. Environmental controls on mid-ocean ridge hydrothermal fluxes. Chem. Geol. 528.
- Coumou, D., Driesner, T., Heinrich, C., 2008. The structure and dynamics of mid-ocean ridge hydrothermal systems. Science 321 (5897), 1825–1828.
- Coumou, D., Driesner, T., Weis, P., Heinrich, C.A., 2009. Phase separation, brine formation, and salinity variation at Black Smoker hydrothermal systems. J. Geophys. Res. 114 (B3).
- Delaney, J., Chave, A., Heath, G.R., Howe, B., Beauchamp, P., 2001. Neptune: real-time, long-term ocean and earth studies at the scale of a tectonic plate. In: OCEANS, MTS/IEEE Conference and Exhibition. Citeseer.
- Delaney, J.R., Robigou, V., McDuff, R.E., Tivey, M.K., 1992. Geology of a vigorous hydrothermal system on the Endeavour segment, juan de Fuca ridge. J. Geophys. Res. 97 (B13), 19663–19682.
- Delaney, J.R., Spiess, F.N., Solomon, S.C., Hessler, R., Karsten, J.L., Baross, J.A., Holcomb, R.T., Norton, D., McDuff, R.E., Sayles, F., 1987. Scientific rationale for establishing long-term ocean bottom observatory/laboratory systems. Mar. Miner. 389–411. Springer.
- Ding, K., Seyfried Jr., W.E., 1992. Determination of Fe-Cl complexing in the low pressure supercritical region (NaCl fluid) - iron solubility constraints on pH of subseafloor hydrothermal fluids. Geochem. Cosmochim. Acta 56 (10), 3681–3692.
- Ding, K., Seyfried Jr., W.E., 1995. In-situ measurement of dissolved H₂ in aqueous fluids at elevated temperatures and pressures. Geochem. Cosmochim. Acta 59, 4769–4773.
- Ding, K., Seyfried Jr., W.E., 1996. Direct pH measurement of NaCl-bearing fluid with an in situ sensor at 400°C and 40 megapascals. Science 272 (5268), 1634–1636.
- Ding, K., Seyfried Jr., W.E., 2007. In-situ measurement of pH and dissolved H₂ in midocean hydrothermal fluids at elevated temperatures and pressures. Chem. Rev. 107 (2), 601–623.
- Ding, K., Seyfried Jr., W.E., Tivey, M.K., Bradley, A.M., 2001. In-situ measurement of dissolved H₂ and H₂S in high-temperature hydrothermal vent fluids at the Main Endeavour Field, Juan de Fuca Ridge. Earth Planet Sci. Lett. 186, 417–425.
- Ding, K., Seyfried Jr., W.E., Tivey, M.K., Von Damm, K.L., Bradley, A.M., Zhang, Z., 2005. In-situ pH measurement of hydrothermal fluids at mid-ocean ridges. Earth Planet Sci. Lett. 237, 167–174.
- Douglas, P.M., Stolper, D.A., Eiler, J.M., Sessions, A.L., Lawson, M., Shuai, Y., Bishop, A., Podlaha, O.G., Ferreira, A.A., Neto, E.V.S., 2017. Methane clumped isotopes: progress and potential for a new isotopic tracer. Org. Geochem. 113, 262–282.
- Driesner, T., Heinrich, C.A., 2007. The system H2O–NaCl. Part I: correlation formulae for phase relations in temperature–pressure–composition space from 0 to 1000°C, 0 to 5000bar, and 0 to 1 XNaCl. Geochem. Cosmochim. Acta 71 (20), 4880–4901.
- Edwards, M.H., Kurras, G.J., Tolstoy, M., Bohnenstiehl, D.R., Coakley, B.J., Cochran, J. R., 2001. Evidence of recent volcanic activity on the ultraslow-spreading Gakkel ridge. Nature 409 (6822), 808–812.
- Elderfield, H., Schultz, A., 1996. Mid-ocean ridge hydrothermal fluxes and the chemical composition of the ocean. Annu. Rev. Earth Planet Sci. 24 (1), 191–224.
- Fontaine, F.J., Wilcock, W.S.D., Foustoukos, D.E., Butterfield, D.A., 2009. A Si-Cl geothermobarometer for the reaction zone of high-temperature, basaltic-hosted midocean ridge hydrothermal systems. G-cubed 10.
- Fornari, D., Von Damm, K., Bryce, J., Cowen, J., Ferrini, V., Fundis, A., Lilley, M., Luther, G., Mullineaux, L., Perfit, M., Meana-Prado, M.F., Rubin, K., Seyfried Jr., W. E., Shank, T., Soule, S.A., Tolstoy, M., White, S., 2012. the East pacific rise between

- 9°N and 10°N: twenty-five years of integrated, multidisciplinary oceanic spreading center studies. Oceanography 25 (1), 18–43.
- Fournier, R.O., 1983. A method of calculating quartz solubilities in aqueous sodium chloride solutions. Geochem. Cosmochim. Acta 47 (3), 579–586.
- Foustoukos, D.I., James, R.H., Berndt, M.E., Seyfried Jr., W.E., 2004. Lithium isotopic systematics of hydrothermal vent fluids at the Main Endeavour Field, northern Juan de Fuca Ridge. Chem. Geol. 212 (1–2), 17–26.
- Foustoukos, D.I., Pester, N.J., Ding, K., Seyfried Jr., W.E., 2009. Dissolved carbon species in associated diffuse and focused flow hydrothermal vents at the Main Endeavour Field, Juan de Fuca Ridge: phase equilibria and kinetic constraints. G-cubed 10.
- Foustoukos, D.I., Seyfried Jr., W.E., 2007. Fluid phase separation processes in submarine hydrothermal systems. In: Liebscher, A., Heinrich, C.A. (Eds.), Fluid-Fluid Interactions, pp. 213–239.
- Gartman, A., Findlay, A.J., Hannington, M., Garbe-Schönberg, D., Jamieson, J.W., Kwasnitschka, T., 2019. The role of nanoparticles in mediating element deposition and transport at hydrothermal vents. Geochem. Cosmochim. Acta 261, 113–131.
- Geiger, S., Driesner, T., Heinrich, C.A., Matthäi, S.K., 2006. Multiphase thermohaline convection in the earth's crust: I. A new finite element – finite volume solution technique combined with a new equation of state for NaCl–H2O. Transport Porous Media 63 (3), 399–434.
- German, C.R., Seyfried, W.E., 2014. Hydrothermal Processes, pp. 191-233.
- Hanor, J.S., 2000. Barite-celestine geochemistry and environments of formation. Rev. Mineral. Geochem. 40 (1), 193–275.
- Hooft, E.E.E., Patel, H., Wilcock, W., Becker, K., Butterfield, D., Davis, E., Dziak, R., Inderbitzen, K., Lilley, M., McGill, P., Toomey, D., Stakes, D., 2010. A seismic swarm and regional hydrothermal and hydrologic perturbations: the northern Endeavour segment, February 2005. G-cubed 11.
- Hsieh, Y.T., Bridgestock, L., Scheuermann, P.P., Seyfried Jr., W.E., Henderson, G.M., 2021. Barium isotopes in mid-ocean ridge hydrothermal vent fluids: a source of isotopically heavy Ba to the ocean. Geochem. Cosmochim. Acta 292, 348–363.
- Ingebritsen, S.E., Geiger, S., Hurwitz, S., Driesner, T., 2010. Numerical simulation of magmatic hydrothermal systems. Rev. Geophys. 48 (1).
- Isern, A.R., Clark, H.L., 2003. the Ocean observatories initiative: a continued presence for interactive ocean research. Mar. Technol. Soc. J. 37 (3), 26–41.
- Jamieson, J.W., Hannington, M.D., Tivey, M.K., Hansteen, T., Williamson, N.M.-B., Stewart, M., Fietzke, J., Butterfield, D., Frische, M., Allen, L., 2016. Precipitation and growth of barite within hydrothermal vent deposits from the Endeavour Segment, Juan de Fuca Ridge, Geochem, Cosmochim, Acta 173, 64–85.
- Janecky, D.R., Seyfried Jr., W.E., 1984. Formation of massive sulfide deposits on oceanic ridge crests: incremental reaction models for mixing between hydrothermal solutions and seawater. Geochem. Cosmochim. Acta 48, 2723–2738.
- Kelley, D., Delaney, J., Juniper, S., 2014. Establishing a new era of submarine volcanic observatories: cabling axial seamount and the Endeavour segment of the juan de Fuca ridge. Mar. Geol. 352.
- Kelley, D.S., Carbotte, S.M., Caress, D.W., Clague, D.A., Delaney, J.R., Gill, J.B., Hadaway, H., Holden, J.F., Hooft, E.E.E., Kellogg, J.P., Lilley, M.D., Stoermer, M., Toomey, D., Weekly, R., Wilcock, W.S.D., 2012. Endeavour segment of the juan de Fuca ridge: one of the most remarkable places on earth. Oceanography 25, 44–61.
- Larson, B., Olson, E., Lilley, M., 2007. In situ measurement of dissolved chloride in high temperature hydrothermal fluids. Geochem. Cosmochim. Acta 71 (10), 2510–2523.
- Liebscher, A., Heinrich, C.A., 2007. Fluid-fluid interactions in the earth's lithosphere. Fluid-Fluid Interact. 65, 1–13.
- Lilley, M.D., Butterfield, D.A., Lupton, J.E., Olson, E.J., 2003. Magmatic events can produce rapid changes in hydrothermal vent chemistry. Nature 422 (6934), 878.
- Lilley, M.D., Butterfield, D.A., Olson, E.J., Lupton, J.E., Macko, S.A., McDuff, R.E., 1993. Anomolous CH₄ and NH₄ concentrations at an unsedimented mid-ocean ridge hydrothermal system. Nature 364, 45–47.
- Lutz, R.A., Shank, T.M., Fornari, D.J., Haymon, R.M., Lilley, M.D., Von Damm, K.L., Desbruyeres, D., 1994. Rapid growth at deep-sea vents. Nature 371 (6499), 663–664.
- Monnin, C., 1999. A thermodynamic model for the solubility of barite and celestite in electrolyte solutions and seawater to 200 degrees C and to 1 kbar. Chem. Geol. 153 (1-4). 187–209.
- Monnin, C., Balleur, S., Goffe, B., 2003. A thermodynamic investigation of barium and calcium sulfate stability in sediments at an oceanic ridge axis (Juan de Fuca, ODP legs 139 and 169). Geochem. Cosmochim. Acta 67 (16), 2965–2976.
- Mullineaux, L.S., Adams, D.K., Mills, S.W., Beaulieu, S.E., 2010. Larvae from Afar colonize deep-sea hydrothermal vents after a catastrophic eruption. Proc. Natl. Acad. Sci. Unit. States Am. 107 (17), 7829–7834.
- Mullineaux, L.S., Peterson, C.H., Micheli, F., Mills, S.W., 2003. Successional mechanism varies along a gradient in hydrothermal fluid flux at deep-sea vents. Ecol. Monogr. 73 (4), 523–542.
- Owens, D., Abeysirigunawardena, D., Biffard, B., Chen, Y., Conley, P., Jenkyns, R., Kerschtien, S., Lavallee, T., MacArthur, M., Mousseau, J., 2022. The oceans 2.0/3.0 data management and archival system. Front. Mar. Sci. 172.
- Pester, N., Rough, M., Ding, K., Seyfried Jr., W.E., 2011. A new Fe/Mn geothermometer for hydrothermal systems: implications for high-salinity fluids at 13°N on the East Pacific Rise. Geochem. Cosmochim. Acta 75, 7881–7892.
- Pester, N.J., Ding, K., Seyfried Jr., W.E., 2015. Vapor-liquid partitioning of alkaline earth and transition metals in NaCl-dominated hydrothermal fluids: an experimental study from 360 to 465 degrees C, near-critical to halite saturated conditions. Geochem. Cosmochim. Acta 168, 111–132.
- Pester, N.J., Reeves, E.P., Rough, M.E., Ding, K., Seewald, J.S., Seyfried Jr., W.E., 2012. Subseafloor phase equilibria in high-temperature hydrothermal fluids of the lucky strike seamount (Mid-Atlantic ridge, 37°17′N). Geochem. Cosmochim. Acta 90, 303–322.

- Rouxel, O., Shanks, W.C., Bach, W., Edwards, K.J., 2008. Integrated Fe- and S-isotope study of seafloor hydrothermal vents at East Pacific rise 9-10°N. Chem. Geol. 252 (3–4), 214–227.
- Scheuermann, P.P., Tan, C., Seyfried Jr., W.E., 2018. Quartz solubility in the two-phase region of the NaCl-H2O system: an experimental study with application to the piccard hydrothermal field, mid-cayman rise. G-cubed 19 (9), 3570–3582.
- Scott, S., Driesner, T., Weis, P., 2017. Boiling and condensation of saline geothermal fluids above magmatic intrusions. Geophys. Res. Lett. 44 (4), 1696–1705.
- Seewald, J.S., Cruse, A., Saccocia, P., 2003. Aqueous volatiles in hydrothermal fluids from the Main Endeavour Field, northern Juan de Fuca Ridge: temporal variability following earthquake activity. Earth Planet Sci. Lett. 216, 575–590.
- Seewald, J.S., Doherty, K.W., Hammar, T.R., Liberatore, S.P., 2002. A new gas-tight isobaric sampler for hydrothermal fluids. Deep Sea Res. Oceanogr. Res. Pap. 49 (1), 189–196.
- Seewald, J.S., Seyfried Jr., W.E., 1990. The effect of temperature on metal mobility in subseafloor hydrothermal systems: constraints from basalt alteration experiments. Earth Planet Sci. Lett. 101 (2–4), 388–403.
- Seyfried Jr., W.E., Bischoff, J.L., 1979. Low temperature basalt alteration by sea water: an experimental study at 70°C and 150°C. Geochem. Cosmochim. Acta 43 (12), 1937–1947
- Seyfried Jr., W.E., Bischoff, J.L., 1981. Experimental seawater-basalt interaction at 300°C, 500 bars, chemical exchange, secondary mineral formation and implications for the transport of heavy metals. Geochem. Cosmochim. Acta 45, 135–149.
- Seyfried Jr., W.E., Ding, K., 1995. Phase equilibria in subseafloor hydrothermal systems: a review of the role of redox, temperature, pH and dissolved Cl on the chemistry of hot spring fluids at mid-ocean ridges. In: Humphris, S.E., Zierenberg, R.A., Mullineaux, L.S., Thompson, R.E. (Eds.), Seafloor Hydrothermal Systems: Physical, Chemical, Biologic and Geological Interactions. American Geophysical Union, pp. 248–273.
- Seyfried Jr., W.E., Pester, N.J., Tutolo, B.M., Ding, K., 2015. The Lost City hydrothermal system: constraints imposed by vent fluid chemistry and reaction path models on subseafloor heat and mass transfer processes. Geochem. Cosmochim. Acta 163, 59–79.
- Seyfried Jr., W.E., Seewald, J.S., Berndt, M.E., Ding, K., Foustoukos, D., 2003. Chemistry of hydrothermal vent fluids from the Main Endeavour field, northern juan de Fuca ridge: geochemical controls in the aftermath of June 1999 seismic events.

 J. Geophys. Res. 108, 2429–2449.
- Shank, T., Fornari, D., Von Damm, K.L., Lilley, M., Haymon, R., Lutz, R.A., 1998. Temporal and spatial patterns of biological community development at nascent deep-seas hydrothermal vents (9°50'N, East Pacific Rise). Deep-Sea Res. II 45, 465–515.
- Shank, T.M., Fornari, D.J., Haymon, R.M., Lilley, M.D., Von Damm, K.L.,
 Desbruyeres, D., 1994. Rapid growth at deep-sea vents. Nature 371 (6499),
 663–664.
- Shikazono, N., 1994. Precipitation mechanisms of barite in sulfate-sulfide deposits in back-arc basins. Geochem. Cosmochim. Acta 58 (10), 2203–2213.
- Sohn, R.A., Fornari, D.J., Von Damm, K.L., Hildebrand, J.A., Webb, S.C., 1998. Seismic and hydrothermal evidence for a cracking event on the East Pacific Rise crest at 9 degrees 50'N. Nature (London) 396 (6707), 159–161.
- Tolstoy, M., Cowen, J.P., Baker, E.T., Fornari, D.J., Rubin, K.H., Shank, T.M., Waldhauser, F., Bohnenstiehl, D.R., Forsyth, D.W., Holmes, R.C., Love, B., Perfit, M. R., Weekly, R.T., Soule, S.A., Glazer, B., 2006. A sea-floor spreading event captured by seismometers. Science 314 (5807), 1920–1922.
- Tolstoy, M., Waldhauser, F., Bohnenstiehl, D.R., Weekly, R.T., Kim, W.Y., 2008. Seismic identification of along-axis hydrothermal flow on the East pacific rise. Nature 451 (7175) 181–184
- Van Ark, E.M., Detrick, R.S., Canales, J.P., Carbotte, S.M., Harding, A.J., Kent, G.M., Nedimovic, M.R., Wilcock, W.S.D., Diebold, J.B., Babcock, J.M., 2007. Seismic structure of the Endeavour segment, juan de Fuca ridge: correlations with seismicity and hydrothermal activity. J. Geophys. Res. Solid Earth 112 (B2).
- Von Damm, K.L., 1995. Controls on the chemistry and temporal variability of seafloor hydrothermal fluids. In: Humphris, S.E., Zierenberg, R.A., Mullineaux, L.S., Thompson, R.E. (Eds.), Seafloor Hydrothermal Systems: Physical, Chemical, Biologic and Geologic Interactions. American Geophysical Union, pp. 222–248.
- Von Damm, K.L., 2000. Chemistry of hydrothermal vent fluids from 9° -10° N, East Pacific Rise; "time zero," the immediate posteruptive period. J. Geophys. Res. 105 (5), 11203–11222.
- Von Damm, K.L., Bischoff, J.L., Rosenbauer, R.J., 1991. Quartz solubility in hydrothermal seawater; an experimental study and equation describing quartz solubility for up to 0.5 M NaCl solutions. Am. J. Sci. 291 (10), 977–1007.
- Von Damm, K.L., Buttermore, L.G., Oosting, S.E., Bray, A.M., Fornari, D.J., Lilley, M.D., Shanks III, W.C., 1997. Direct observation of the evolution of a seafloor "black smoker" from vapor to brine. Earth Planet Sci. Lett. 149, 101–111.
- Von Damm, K.L., Edmond, J.M., Measures, C.I., Grant, B., 1985. Chemistry of submarine hydrothermal solutions at guaymas basin, gulf of California. Geochem. Cosmochim. Acta 49 (11), 2221–2237.
- Von Damm, K.L., Lilley, M., Shanks, W.C., Brockington, M., Bray, A., O'Grady, K.M., Olson, E., Graham, A., Proskurowski, G., 2003. Extraordinary phase separation and segregation in vent fluids from the southern East Pacific Rise. Earth Planet Sci. Lett. 206. 365–378.
- Von Damm, K.L., Lilley, M.D., 2004. Diffuse flow hydrothermal fluids from 9⁰ 50' N East Pacific Rise: origin, evolution and biogeochemical controls. The Subseafloor Biosph. Mid-Ocean Rid. 144, 245–268.
- Wilcock, W.S., Archer, S.D., Purdy, G., 2002. Microearthquakes on the Endeavour segment of the juan de Fuca ridge. J. Geophys. Res. Solid Earth 107 (B12). EPM 4-1-EPM 4-21.

Wilcock, W.S., Hooft, E.E.E., Toomey, D.R., McGill, P.R., Barclay, A.H., Stakes, D.S., Ramirez, T.M., 2009. The role of magma injection in localizing black-smoker activity. Nat. Geosci. 2 (7), 509–513.

Wilcock, W.S., McNabb, A., 1996. Estimates of permeability on the Endeavour segment of the Juan de Fuca mid-ocean ridges. Earth Planet Sci. Lett. 138, 83–91.
Wu, S.-j., Yang, C.-j., Ding, K., Tan, C.-y., 2015. A remotely operated serial sampler for collecting gas-tight fluid samples. China Ocean Eng. 29 (5), 783–792.